Universität des Saarlandes

Fachrichtung 6.1 – Mathematik

Preprint Nr. 220

PDE-based Morphology for Matrix Fields: Numerical Solution Schemes

Bernhard Burgeth, Michael Breuß,
Stephan Didas and Joachim Weickert

Saarbrücken 2007

Fachrichtung 6.1 – Mathematik
Universität des Saarlandes

Preprint No. 220
submitted: September 17, 2008

PDE-based Morphology for Matrix Fields: Numerical Solution Schemes

Bernhard Burgeth
Saarland University
Department of Mathematics and Computer Science
P.O. Box 15 11 50
66041 Saarbrücken
Germany
burgeth@mia.uni-saarland.de

Michael Breuß
Saarland University
Department of Mathematics and Computer Science
P.O. Box 15 11 50
66041 Saarbrücken
Germany
bebe@domain.de

Stephan Didas
Saarland University
Department of Mathematics and Computer Science
P.O. Box 15 11 50
66041 Saarbrücken
Germany
didas@mia.uni-saarland.de

Joachim Weickert
Saarland University
Department of Mathematics and Computer Science
P.O. Box 15 11 50
66041 Saarbrücken
Germany
weickert@mia.uni-saarland.de

Edited by
FR 6.1 – Mathematik
Universität des Saarlandes
Postfach 15 11 50
66041 Saarbrücken
Germany

Fax: + 49 681 302 4443
e-Mail: preprint@math.uni-sb.de
WWW: http://www.math.uni-sb.de/

Abstract

Tensor fields are important in digital imaging and computer vision. Hence there is a demand for morphological operations to perform e.g. shape analysis, segmentation or enhancement procedures. Recently, fundamental morphological concepts have been transferred to the setting of fields of symmetric positive definite matrices, which are symmetric rank two tensors. This has been achieved by a matrix-valued extension of the nonlinear morphological partial differential equations (PDEs) for dilation and erosion known for grey scale images. Having these two basic operations at our disposal, more advanced morphological operators such as top hats or morphological derivatives for matrix fields with symmetric, positive semidefinite matrices can be constructed. The approach realises a proper coupling of the matrix channels rather than treating them independently. However, from the algorithmic side the usual scalar morphological PDEs are transport equations that require special upwind-schemes or novel high-accuracy predictor-corrector approaches for their adequate numerical treatment. In this chapter we propose the non-trivial extension of these schemes to the matrix-valued setting by exploiting the special algebraic structure available for symmetric matrices. Furthermore we compare the performance and juxtapose the results of these novel matrix-valued high-resolution-type (HRT) numerical schemes by considering top hats and morphological derivatives applied to artificial and real world data sets.

1 Introduction

Initiated by Serra's and Matheron's work on binary morphology [33, 46] in the sixties, mathematical morphology has developed into a powerful discipline that provides versatile tools to the image processing community. Over the last four decades morphological concepts have been generalised and extended not only to greyscale images but also to vector-valued images and image sequences. Numerous monographs, e.g. [26, 34, 47, 48, 51], and conference proceedings, e.g. [21, 22, 27, 32, 53], bear testimony to the variety and the success of mathematical morphology.

Recently, the fundamental morphological operations of dilation and erosion, and with it some other basic morphological operators, have been made available for matrix-valued data, *matrix fields* for short [11].

The interest of the image processing community in matrix-valued data has been triggered mainly by the advent of diffusion tensor magnetic resonance imaging (DT-MRI) [3]. This 3-D medical imaging technique assigns to each

voxel a tensor, i. e., a positive semidefinite 3×3-matrix, which provides in vivo information about the diffusion of water molecules in biological tissue. As such it mirrors the geometry and organisation of the tissue under examination and is a very valuable diagnostic tool [39]. Furthermore, in image analysis itself tensors turned out to be a useful concept [23]: The *structure tensor* [18], for instance, (also known as Förstner interest operator, second moment matrix or scatter matrix) is used for corner detection [25], but also for motion [4] and texture analysis [40]. Finally, in physics and engineering anisotropic behaviour of quantities is described by tensors such as inertia, diffusion, permittivity and stress-strain tensors. Hence, modern image processing should provide appropriate tools to analyse matrix fields.
To fix notation we consider a matrix field as a mapping

$$F : \Omega \subset \mathbb{R}^d \longrightarrow M_n(\mathbb{R}) \tag{1}$$

from a d-dimensional image domain into the set of $k \times k$-matrices with real entries, $F(x) = (f_{p,q}(x))_{p,q=1,\ldots,n}$. Unless otherwise stated we will concentrate throughout this chapter on matrix fields with values in the set $\mathrm{Sym}(k)$ of all *symmetric* matrices, $\mathrm{Sym}(k) \subset M_k(\mathbb{R})$. In most applications this type of matrices is of practical relevance.
In [10] novel matrix-valued partial differential equations governing dilation and erosion for matrix fields have been proposed and numerically solved by a first-order scheme of Osher and Sethian generalised to the setting of matrices. However, in the case of scalar images the morphological differential equations of dilation and erosion can also be solved numerically by a flux corrected transport (FCT) scheme as introduced in [8]. This scheme follows a predictor-corrector strategy which allows for an almost perfect preservation of edges and discontinuities outperforming even a high-resolution scalar variant of the Osher-Sethian scheme. In what follows, we denote the corresponding Osher-Sethian schemes by OS-I and OS-II, respectively.
As a novelty we propose in this chapter high-resolution-type matrix-valued extensions of OS-II as well as of the FCT scheme. Furthermore, we compare in experiments on matrix fields the performance of OS-I, OS-II, FCT, and we juxtapose the results to the output of the ordering based morphological operators which were introduced and investigated in [15, 12].
The paper has the following structure: First we deal in Section 2 with mathematical morphology for grey scale images. We present the ordering and the PDE-based approach for the two fundamental operations, dilation and erosion. For the nonlinear hyperbolic PDEs governing dilation and erosion we present three schemes for their numerical solution. The section ends with a short review of some basic morphological derivative operators. Section 3

gives a compact description how the operations of dilation and erosion can be defined for matrix fields. To this end we utilise the Loewner partial ordering for symmetric matrices to define a supremum and infimum of a finite set of symmetric matrices. In Section 4 we establish matrix-valued PDEs for dilation and erosion, and we introduce matrix-valued counterparts of the three schemes for the numerical solution of the dilation/erosion equations in the setting of matrix fields. In our experiments we apply morphological operations to artificial and real DT-MRI data sets. The operations are realised via ordering and via the three numerical schemes of the PDE-based approach. We report on the comparison of the results in Section 5. The remarks in Section 6 conclude this chapter.

2 Morphology for Greyscale Images

In this section we briefly recall the definitions of some basic scalar-valued morphological operators whose matrix-valued generalisations will be of interest in this chapter. First we focus on the two very different approaches to the fundamental operations of mathematical morphology: Dilation and erosion.
The first approach is based on ordering leading to the so-called flat morphology while the continuous-scale morphology relies on partial differential equations. After introducing these approaches, we briefly recall some important morphological operations based on subsequent applications of dilation/erosion.
A second topic addressed here are numerical schemes for scalar-valued PDE-based morphology. After a general discussion, we introduce the methods we use in this paper, giving them a formulation easily carried over to the tensor-valued setting discussed later.

2.1 Erosion and dilation based on ordering

In flat morphology for a scalar image $f(x, y)$ the so-called *structuring element* (SE) is a set $B \subset \mathbb{R}^2$ that determines the neighbourhood relation of pixels with respect to a shape analysis task. Often convex sets such as disks, ellipses or squares are used as structuring elements.
Grey scale *dilation* $\oplus$ replaces the greyvalue of the image $f(x, y)$ by its supremum/maximum within a mask defined by B,

$$(f \oplus B)\,(x, y) \;:=\; \sup\,\{f(x-x',\, y-y') \mid (x', y') \in B\}, \tag{2}$$

while *erosion* $\ominus$ is determined by taking the infimum/minimum,

$$(f \ominus B)\,(x,y) \;:=\; \inf\,\{f(x{+}x',\, y{+}y') \mid (x',y') \in B\}. \tag{3}$$

The notions of supremum and infimum only make sense if an ordering of the grey values is possible. The following PDE-based approach is in principle free from this requirement.

2.2 Erosion and dilation by PDEs

In ([43, 44]) nonlinear partial differential equations were proposed that mimic the process of dilation and erosion of an image f with a ball as structuring element. These Eikonal equations read

$$\begin{aligned} \partial_t u &= \pm\,\|\nabla u\| := \sqrt{(\partial_x u)^2 + (\partial_y u)^2} \quad \text{on} \quad \Omega\times]0,+\infty[\\ \partial_n u &= 0 \quad \text{on} \quad \partial\Omega\times]0,+\infty[\\ u(x,y,0) &= f(x,y) \quad \text{for all} \quad (x,y)\in\Omega \end{aligned} \tag{4}$$

The evolution process governed by (4) is initialised with the original image f and yields transformed versions $u(\cdot,t)$ for any $t \in]0,+\infty[$. Here $\partial_n u$ denotes the outward normal derivative of u at the boundary $\partial\Omega$ of the image domain Ω. The plus sign $+$ realises the dilation, while the minus sign $-$ corresponds to erosion.
The dilation/erosion PDEs (4) belong to the class of *hyperbolic* PDEs, see e.g. [16, 17] for introduction. Hyperbolic processes describe transport processes and are strongly linked to wave propagation. An important property of solutions to hyperbolic PDEs is that discontinuities, often called *shocks*, generally arise. Note in the context of this work, that the resolution of shocks requires specifically tailored numerical schemes, see e.g. [31].

2.3 Morphological operations

The combination of dilation and erosion lead to various other morphological operators such as *opening* and *closing*,

$$f \circ B := (f \ominus B) \oplus B\,, \qquad f \bullet B := (f \oplus B) \ominus B\,, \tag{5}$$

the *white top-hat* and its dual, the *black top-hat*,

$$\mathrm{WTH}(f) := f - (f \circ B)\,, \qquad \mathrm{BTH}(f) := (f \bullet B) - f\,, \tag{6}$$

and finally, the *self-dual top-hat*,

$$\mathrm{SDTH}(f) := (f \bullet B) - (f \circ B)\,. \tag{7}$$

Boundaries of objects are loci of high grey value variations in an image, and as such they can be detected by derivative operators. The so-called *Beucher gradient*

$$\varrho_B(f) := (f \oplus B) - (f \ominus B)\,, \tag{8}$$

as well as the *internal* and *external gradient*,

$$\varrho_B^-(f) := f - (f \ominus B)\,, \qquad \varrho_B^+(f) := (f \oplus B) - f\,, \tag{9}$$

are morphological counterparts of the norm of the gradient f, $\|\nabla f\|$, if f is considered as a differentiable image.
In [55] a *morphological Laplacian* has been introduced. But we define a variant by

$$\Delta_B f := \varrho_B^+(f) - \varrho_B^-(f) = (f \oplus B) - 2 \cdot f + (f \ominus B)\,. \tag{10}$$

This Laplacian is a morphological equivalent of the second derivative $\partial_{\eta\eta} f$ where η stands for the unit vector in the direction of the steepest slope. It allows us to distinguish between influence zones of minima and maxima of the image f. This is a vital property for the construction of so-called *s*hock filters [24, 30, 37]. Shock filtering amounts to applying either a dilation or an erosion to an image, depending on whether the pixel is located within the influence zone of a minimum or a maximum:

$$S_B f := \begin{cases} f \oplus B\,, & \Delta_B f < 0, \\ f\,, & \Delta_B f = 0, \\ f \ominus B\,, & \Delta_B f > 0. \end{cases} \tag{11}$$

A considerable number of variants of shock filters have been considered in the literature [1, 20, 36, 41, 45, 56]. When they are applied iteratively, experiments show that their steady state is given by a piecewise constant image with discontinuities ("shocks") between adjacent segments of constant grey value. For more details about the morphological shock filter as introduced above see [12].

These operators are at our disposal once we have succeeded to performing dilation and erosion on matrix fields. Depending on the quality of the discrete realisations these two operations we will see considerable differences in the output of the composed morphological operators.

2.4 Numerical schemes for PDEs of erosion or dilation

In the context of PDE-based mathematical morphology, first-order finite difference methods such as the *Osher-Sethian scheme* [35, 38, 49] and the *Rouy-Tourin method* [42, 54] are adequate choices. A typical design feature of such

PDE-based algorithms for mathematical morphology consists of diffusive numerical effects necessary to capture propagating shocks. Unfortunately, this also leads to a blurring of edges.
The construction of an accurate method yielding sharp edges is a non-trivial task. In [50, 52], the attempt to circumvent this blurring by means of using higher-order ENO[1] interpolants within numerical schemes was investigated in scalar-valued morphology. However, schemes like these are very difficult to implement in a tensor-valued setting since the mathematical concept behind ENO interpolants does not carry over. On the other hand, as we show in this work, it is possible to define a reasonable tensor-valued analogue of the high-resolution extension of the first-order Osher-Sethian scheme, and also the *flux-corrected transport (FCT)* scheme introduced in [8] for scalar-valued morphology can be extended to the tensor-valued setting. Consequently, we denote the resulting schemes as being of *high-resolution-type (HRT)*, and these are to the knowledge of the authors the first schemes in the area of tensor-valued data constructed for the purpose of a high-quality resolution.

In this section, we briefly review the first-order Osher-Sethian scheme (OS-I) as well as its high-resolution extension (OS-II), and the FCT scheme for the scalar-valued 2-D case. Restricting the presentation to this setting, all numerical aspects will become evident while the notation is not overloaded. We employ the notation u_{ij}^n as the grey value of the image u at the pixel centred at $(ih_x, jh_y) \in \mathbb{R}^2$ at the time-level $n\tau$ of the evolution. For the convenience of the reader, the formulae are already given in a format so that the coding procedure is extendable to the 3-D tensor-valued setting in a straightforward fashion:

- Instead of grey values u_{ij}^n the reader may employ tensors $U^n(ih_x, jh_y)$.
- Instead of the minmod-function defined below in a scalar-valued setting, the reader may employ its tensor-valued generalisation discussed in Paragraph 4.
- The formulae can be extended straightforwardly to tensors in 3-D $U^n(ih_x, jh_y, kh_z)$.

Also, we only describe the schemes for morphological dilation, as algorithms for erosion just incorporate a switch of sign, compare (4).

For a compact notation, we employ the usual abbreviations for forward and backward difference operators, i.e.,

$$D_+^x u_{i,j}^n := u_{i+1,j}^n - u_{i,j}^n \quad \text{and} \quad D_-^x u_{i,j}^n := u_{i,j}^n - u_{i-1,j}^n \,. \tag{12}$$

[1] ENO means *essentially non-oscillatory*

These operators can be defined analogously with respect to the y-direction, and they can be formally concatenated yielding the obvious results. It also turns out to be advantageous to define the central difference operator

$$D_c^x u_{i,j}^n \;:=\; u_{i+1,j}^n - u_{i-1,j}^n \tag{13}$$

which should be understood accordingly.

2.5 The basic Osher-Sethian scheme

The first-order-accurate Osher-Sethian scheme for morphological dilation referred to as OS-I is given by

$$\begin{aligned} u_{i,j}^{n+1} \;=\; u_{i,j}^n \;+\; \tau \Bigg(& \left(\frac{1}{h_x}\min\left(D_-^x u_{i,j}^n, 0\right)\right)^2 + \left(\frac{1}{h_x}\max\left(D_+^x u_{i,j}^n, 0\right)\right)^2 \\ & + \left(\frac{1}{h_y}\min\left(D_-^x u_{i,j}^n, 0\right)\right)^2 + \left(\frac{1}{h_y}\max\left(D_+^x u_{i,j}^n, 0\right)\right)^2 \Bigg)^{1/2} . \end{aligned} \tag{14}$$

The scheme (14) is largely identical to the first-order upwind scheme of Rouy and Tourin [42, 54], but with the exception of the treatment of extrema of $u_{i,j}^n$.

2.6 The Osher-Sethian scheme with high-resolution correction

For notational convenience, we first write down this enhanced scheme, named OS-II, in semidiscrete form keeping the time derivative, compare [38]. Note, that it is at this stage identical to (14) with the exception of terms tweaking the numerical derivatives:

$$\begin{aligned} \frac{\partial}{\partial t} u_{i,j}(t) \;=\; & \Bigg(\left(\frac{1}{h_x}\min\left(D_-^x u_{i,j}^n + \frac{1}{2}\mathrm{mm}\left(D_-^x D_+^x u_{i,j}^n, D_-^x D_-^x u_{i,j}^n\right), 0\right)\right)^2 \\ & + \left(\frac{1}{h_x}\max\left(D_+^x u_{i,j}^n - \frac{1}{2}\mathrm{mm}\left(D_+^x D_+^x u_{i,j}^n, D_-^x D_+^x u_{i,j}^n\right), 0\right)\right)^2 \\ & + \left(\frac{1}{h_y}\min\left(D_-^y u_{i,j}^n + \frac{1}{2}\mathrm{mm}\left(D_-^y D_+^y u_{i,j}^n, D_-^y D_-^y u_{i,j}^n\right), 0\right)\right)^2 \\ & + \left(\frac{1}{h_y}\max\left(D_+^y u_{i,j}^n - \frac{1}{2}\mathrm{mm}\left(D_+^y D_+^y u_{i,j}^n, D_-^y D_+^y u_{i,j}^n\right), 0\right)\right)^2 \Bigg)^{1/2} . \end{aligned} \tag{15}$$

In (15), the function $\mathrm{mm}(\cdot,\cdot)$ denotes the so-called minmod-function defined as

$$\mathrm{mm}(a,b) := \begin{cases} \min(a,b) & \text{if} \quad a>0 \text{ and } b>0\,, \\ \max(a,b) & \text{if} \quad a<0 \text{ and } b<0\,, \\ 0 & \text{else}\ . \end{cases} \tag{16}$$

It is left to define the time stepping method discretising the time derivative in (15), whereby we denote the right hand side of (15) as $L(u^n,i,j)$. This is done by the method of Heun, yielding the final update formula

$$\bar{u}_{i,j}^{n+1} = u_{i,j}^n + \tau\, L(u^n,i,j) \tag{17}$$

$$u_{i,j}^{n+1} = \frac{1}{2}u_{i,j}^n + \frac{1}{2}\bar{u}_{i,j}^{n+1} + \frac{\tau}{2}L\left(\bar{u}^{n+1},i,j\right)\ . \tag{18}$$

2.7 The Rouy-Tourin scheme

Another first-order-accurate scheme has been proposed by Rouy and Tourin in [42]. The variant we employ in this chapter reads

$$u_{i,j}^{n+1} = u_{i,j}^n + \tau \left(\max\left(\frac{1}{h_x}\max\left(-D_-^x u_{i,j}^n, 0\right)\ ,\ \frac{1}{h_x}\max\left(D_+^x u_{i,j}^n, 0\right)\right)^2 + \max\left(\frac{1}{h_x}\max\left(-D_-^y u_{i,j}^n, 0\right)\ ,\ \frac{1}{h_x}\max\left(D_+^y u_{i,j}^n, 0\right)\right)^2\right)^{1/2} \tag{19}$$

It displays a performance very similar to that of the first-order scheme OS-I, hence we refrain from showing experiments based on this scheme alone. However, we use it as a predictor step in the FCT scheme as it will be pointed out in the following subsection.

2.8 The FCT scheme

The FCT scheme summarised below is by construction a new variant of a technique originally proposed by Boris and Book [5, 6, 7] in the context of fluid flow simulation. As shown in [8], the FCT scheme results in accurate and (largely) rotationally invariant discrete representations of continuous-scale morphological dilation/erosion.

The proposed FCT scheme relies on one-sided upwind differences as both schemes previously presented above. Instead of terms refining the gradient approximation as in (15), the idea behind the FCT scheme is to quantify the undesirable blurring effects introduced by upwinding and to negate the corresponding quantity in a corrector step by *stabilised inverse diffusion (SID)*.

Note that due to the stabilisation, the SID process is not ill-posed, compare [9].
In order to define the FCT scheme, let us give the abbreviations

$$\lceil^x u_{i,j}^n := \frac{\tau}{2h_x}\left|D_c^x u_{i,j}^n\right| + \frac{\tau}{2h_x} D_+^x u_{i,j}^n - \frac{\tau}{2h_x} D_-^x u_{i,j}^n\,, \tag{20}$$

$$\lceil^y u_{i,j}^n := \frac{\tau}{2h_y}\left|D_c^y u_{i,j}^n\right| + \frac{\tau}{2h_y} D_+^y u_{i,j}^n - \frac{\tau}{2h_y} D_-^y u_{i,j}^n\,. \tag{21}$$

Let us stress, that the quantities $\lceil^x u_{i,j}^n$ and $\lceil^y u_{i,j}^n$ just describe the upwinding incorporated in (19), see [8] for details. An important observation is, that the central differences above incorporate a second-order error which is non-diffusive, while the one-sided differences are discrete diffusive fluxes. Thus, a spatial discretisation relying on (20)–(21) such as the Rouy-Tourin scheme (19) introduces exactly these diffusive fluxes. The FCT procedure then inverts the corresponding numerical diffusion using the predicted data in the corrector step.
Using the method (19) as a *predictor* denoting the result pointwise as $u_{i,j}^{n+1,\mathrm{pred}}$, we are now concerned with the *corrector step*, which will finally read as

$$u_{ij}^{n+1} = u_{ij}^{n+1,\mathrm{pred}} + q_h^{n+1,\mathrm{pred}} - q_d^{n+1,\mathrm{pred}}\,. \tag{22}$$

The FCT scheme then consists of a subsequent application of (19) and (22). We now define the terms occurring in (22). As indicated, it is essential for the FCT procedure to split the diffusive part from the second-order part. To this end, let us note that the discretisation of the dilation PDE using central differences only,

$$u_{i,j}^{n+1,\mathrm{pred}} = u_{ij}^n + \sqrt{\left(\frac{\tau}{2h_x}\left|D_c^x u_{i,j}^n\right|\right)^2 + \left(\frac{\tau}{2h_y}\left|D_c^y u_{i,j}^n\right|\right)^2}\,, \tag{23}$$

incorporates no numerical diffusion in the spatial discretisation part.
Let us now consider *predicted data* as arguments in the formulae of our numerical schemes. Then, adding zero by adding and subtracting the square root below (23) on the right hand side of (19), we can easily identify the higher-order part $q_h^{n+1,\mathrm{pred}}$ in (22) as

$$q_h^{n+1,\mathrm{pred}} := \sqrt{\left(\frac{\tau}{2h_x}\left|D_c^x u_{i,j}^{n+1,\mathrm{pred}}\right|\right)^2 + \left(\frac{\tau}{2h_y}\left|D_c^y u_{i,j}^{n+1,\mathrm{pred}}\right|\right)^2}\,. \tag{24}$$

For the lower-order term $q_d^{n+1,\mathrm{pred}}$ in (22) we have to take into account the

stabilisation of the backward diffusive fluxes. This is done making use of

$$g_{i+1/2,j} := \mathrm{mm}\left(D_-^x u_{i,j}^{n+1,\mathrm{pred}},\ \frac{\tau}{2h_x} D_+^x u_{i,j}^{n+1,\mathrm{pred}},\ D_+^x u_{i+1,j}^{n+1,\mathrm{pred}} \right), \quad (25)$$

$$g_{i,j+1/2} := \mathrm{mm}\left(D_-^y u_{i,j}^{n+1,\mathrm{pred}},\ \frac{\tau}{2h_y} D_+^y u_{i,j}^{n+1,\mathrm{pred}},\ D_+^y u_{i,j+1}^{n+1,\mathrm{pred}} \right), \quad (26)$$

where $\mathrm{mm}(\cdot,\cdot,\cdot)$ is a straightforward extension of the minmod-function defined in (16) to three arguments. Employing then the stabilised fluxes within the formulae of (20)-(21), but applied at predicted data, we obtain

$$\delta^x u_{i,j}^{n+1,\mathrm{pred}} := \frac{\tau}{2h_x} \left| D_c^x u_{i,j}^{n+1,\mathrm{pred}} \right| + g_{i+1/2,j} - g_{i-1/2,j}, \quad (27)$$

$$\delta^y u_{i,j}^{n+1,\mathrm{pred}} := \frac{\tau}{2h_y} \left| D_c^y u_{i,j}^{n+1,\mathrm{pred}} \right| + g_{i,j+1/2} - g_{i,j-1/2}\,, \quad (28)$$

yielding the second new term in (22) as

$$q_d^{n+1,\mathrm{pred}} := \sqrt{\left(\delta^x u_{i,j}^{n+1,\mathrm{pred}}\right)^2 + \left(\delta^y u_{i,j}^{n+1,\mathrm{pred}}\right)^2}\,. \quad (29)$$

We now conclude our review of morphology in the scalar setting and proceed with the transfer to the matrix-valued case.

3 Ordering Based Morphology for Matrix Fields

Since dilation resp. erosion of flat morphology are defined via supremum and infimum, see (2) and (3), a suitable ordering on the set of image values is necessary. Dealing with symmetric matrices as image values the so-called *Loewner ordering* is a natural choice. We introduce this partial ordering and other useful concepts from matrix analysis in the next subsection.

3.1 Matrix Analysis

Of particular importance for us is the subset $\mathrm{Sym}(k)$ of symmetric $k \times k$-matrices with real entries. They form a vector space endowed with the scalar product

$$\langle A, B \rangle := \sqrt{\mathrm{trace}(A^\top B)}\,. \quad (30)$$

Note that at each point the matrix $F(x)$ of a field of symmetric matrices can be diagonalised and decomposed into its spectral components yielding

$$F(x) = V(x)^\top D(x) V(x) = \sum_{i=1}^{n} \lambda_i(x)\ v_i(x) v_i^\top(x)\,. \quad (31)$$

Here $V(x) \in \mathcal{O}(k)$ is a matrix field of orthogonal matrices $V(x)$ with column vectors $v_i(x)$, $i = 1, \ldots, n$, while $D(x)$ is a matrix field of diagonal matrices with entries $\lambda_i(x)$, $i = 1, \ldots, n$. In the sequel we will denote $n \times n$ - diagonal matrices with entries $\lambda_1, \ldots, \lambda_n \in \mathbb{R}$ from left to right simply by $\operatorname{diag}(\lambda_1, \ldots, \lambda_n)$, and $\mathcal{O}(k)$ stands for the matrix group of orthogonal $n \times n$-matrices.
We need to define functions h of symmetric matrices. The most common way to do this is as follows [29]. Let $\operatorname{diag}(\alpha_1, \ldots, \alpha_n)$ denote a diagonal matrix with entries $\alpha_1, \ldots, \alpha_n$. We define for a symmetric matrix $A \in \operatorname{Sym}(k)$ with eigenvalue decomposition $A = V \operatorname{diag}(\alpha_1, \ldots, \alpha_n) V^\top$ and orthogonal matrix $V \in \mathcal{O}(k)$ the matrix $h(A)$ by

$$h(A) := V \operatorname{diag}(h(\alpha_1), \ldots, h(\alpha_n)) V^\top \tag{32}$$

provided the α_i's lie in the domain of definition of h. Note that the outcome of that operation is rotational invariant, $h(WAW^\top) = Wh(A)W^\top$, $W \in \mathcal{O}(k)$, and preserves symmetry, $h(A) \in \operatorname{Sym}(k)$.
For example, specifying h as the absolute value function, $h(x) = |x|$, associates with a matrix A its absolute value $|A|$. This $|A|$ denotes a positive semidefinite matrix and must not be confused with the norm or determinant of A.
The set of positive (semi-)definite matrices, denoted by $\operatorname{Sym}^+(k)$ ($\operatorname{Sym}^{++}(k)$, resp.), consists of all symmetric matrices A with $\langle v, Av \rangle := v^\top Av > 0 \quad (\geq 0, \text{ resp.,})$ for $v \in \mathbb{R}^n \setminus \{0\}$.
The set $\operatorname{Sym}^+(k)$ forms a cone, that is, a set that is invariant under addition of matrices as well as multiplication with a positive scalar. This cone is used to define a partial ordering on $\operatorname{Sym}(k)$, the Loewner ordering:

$$A, B \in \operatorname{Sym}(k): \quad A \geq B :\Leftrightarrow A - B \in \operatorname{Sym}^+(k), \tag{33}$$

i. e. $A \geq B$ if and only if $A - B$ is positive semidefinite.
A subset K of a cone C is called *base* if every $y \in C, y \neq 0$ is uniquely representable as $y = r \cdot x$ with $x \in K$ and $r > 0$. For instance, the set of positive semidefinite matrices with trace 1 form a convex and compact base K_1 of $\operatorname{Sym}^+(k)$: $K_1 := \{M \in \operatorname{Sym}^+(k) : \operatorname{trace}(M) = 1\}$.
A point x is an extreme point of a convex subset $S \subset V$ of a vector space V if and only if $S \setminus \{x\}$ is still convex. The set of all extreme points of S is denoted $\operatorname{ext}(S)$.
All the important information of a convex compact set is captured in its extreme points. The theorems of Minkowski and Krein-Milman state that each convex compact set S in a finite dimensional vector space can be reconstructed as the set of all finite convex combinations of its extreme points

[2, 28]:

$$
\begin{aligned}
S &= \text{convexhull}(\text{ext}(S)) \\
&= \left\{ \sum_{i=1}^{N} \lambda_i \, e_i \mid N \in I\!N, e_i \in \text{ext}(S), \lambda_i \geq 0, \text{ for } i = 1, \ldots, N, \ \sum_{i=1}^{N} \lambda_i = 1 \right\}.
\end{aligned}
$$

It is known [2] that the matrices $v\,v^\top$ with unit vectors $v \in \mathbb{R}^n$, $\|v\| = 1$ are exactly the extreme points of a base K_1 of $\text{Sym}^+(k)$. Because of this extremal property the matrices $v\,v^\top$ with $\|v\| = 1$ carry the complete information about the base of the Loewner ordering cone and hence the cone itself: $\text{convexhull}(\{v\,v^\top : v \in \mathbb{R}^n, \|v\| = 1\})$ is a base for the Loewner ordering cone. Such extreme points of bases of translated Loewner cones will play a decisive role in the explicit calculation of the supremum/infimum of a finite number of symmetric matrices.

3.2 Maximal / Minimal Matrices in the Loewner Ordering

The supremum of two symmetric matrices A_1 and A_2 is obtained easily. As it was pointed out in [10] the quantity

$$
\sup(A_1, A_2) \;=\; \frac{1}{2}\,(A_1 + A_2) + \frac{1}{2}\,|A_1 - A_2|\,, \tag{34}
$$

well known to hold for real numbers, indeed provides the supremum of the two matrices with respect to the Loewner ordering. The infimum of two matrices we obtain through

$$
\inf(A_1, A_2) \;=\; \frac{1}{2}\,(A_1 + A_2) - \frac{1}{2}\,|A_1 - A_2|\,. \tag{35}
$$

We will need in Section 5 a minmod-function for matrix fields, and to this end the supremum/infimum of three symmetric matrices A_1, A_2, A_3 has to be calculated. However, the iteration of (34) leads to the upper bounds

$$
\begin{gathered}
S_1 := \sup(A_1, \sup(A_2, A_3))\,, \quad S_2 := \sup(A_2, \sup(A_3, A_1))\,, \\
S_3 := \sup(A_3, \sup(A_1, A_2))\,,
\end{gathered} \tag{36}
$$

for the set $\{A_1, A_2, A_3\}$ that in general do not coincide:

$$
S_1 \neq S_2 \neq S_3\,. \tag{37}
$$

We construct an approximate supremum of $\{A_1, A_2, A_3\}$ in the following manner. Since each S_i dominates $\{A_1, A_2, A_3\}$ so does their arithmetic mean:

$$S_m := \frac{1}{3}(S_1 + S_2 + S_3) \geq A_i, \quad i = 1, 2, 3\,. \tag{38}$$

We can improve this upper bound S_m by finding an optimal $\tau \geq 0$ such that

$$S_m - \tau I \geq A_i, \quad i = 1, 2, 3, \tag{39}$$

holds, where I denotes the identity matrix. If $\mu_{ij} \geq 0$, $j = 1, \ldots, k$, are the eigenvalues of $S_m - A_i$ for $i = 1, 2, 3$, this optimal τ is given by the minimum of all these eigenvalues

$$\tau_{opt} = \min_{\substack{i=1,\ldots,3 \\ j=1,\ldots,k}} (\mu_{ij}) \tag{40}$$

yielding a suitable supremum of three matrices

$$\sup_{opt}(A_1, A_2, A_3) = S_m - \tau_{opt} I\,. \tag{41}$$

The infimum of three matrices is calculated by

$$\inf_{opt}(A_1, A_2, A_3) \;=\; -\sup_{opt}(-A_1, -A_2, -A_3)\,. \tag{42}$$

It is clear that an extension of this approach to four or more matrices is not feasible. To extend the notions of dilation (2) and erosion (3) to matrix fields a different method to calculate the supremum/infimum of a larger number of matrices A_i has to be employed. Such a technique has been developed and described in detail in [10, 12]. However, in order to keep this presentation as self-contained as possible we sketch this approach in the following.
Using the customary notation $a + r\,S := \{a + r \cdot s : s \in S\}$ for a point $a \in V$, a scalar $r \in \mathbb{R}$ and a subset $S \subset V$, we define the *penumbra* $P(M)$ of a matrix $M \in \mathrm{Sym}(k)$ as the set of matrices N that are smaller than M w.r.t. the Loewner ordering:

$$P(M) := \{N \in \mathrm{Sym}(k) : N \leq M\} = M - \mathrm{Sym}^+(k)\,. \tag{43}$$

The penumbra $P(M)$ is a reverted and translated version of the Loewner cone geometrically characterising all matrices that are smaller than the matrix M marking its vertex.
Using this geometric description the problem of finding the maximum of a set of matrices $\{A_1, \ldots, A_m\}$ amounts to determining the minimal penumbra covering their penumbras $P(A_1), \ldots, P(A_m)$. Its vertex represents the matrix supremum $\overline{A} := \sup(A_1, \ldots, A_m)$ we are searching for and that dominates all A_i w.r.t the Loewner ordering.

To this end we associate with each matrix $M \in \mathrm{Sym}(k)$ a *ball* in the subspace $\{A : \mathrm{trace}(A) = 0\}$ of all matrices with zero trace as a *completely descriptive set*. For the sake of simplicity we will assume that $\mathrm{trace}(M) \geq 0$. We determine the center and the radius of this enclosing ball: First, we note that the set $\big\{M - \mathrm{trace}(M) \cdot \mathrm{convexhull}\{v\,v^\top : v \in \mathbb{R}, \|v\| = 1\}\big\}$ is a base for $P(M)$ contained in the subspace $\{A : \mathrm{trace}(A) = 0\}$. The orthogonal projection of M onto $\{A : \mathrm{trace}(A) = 0\}$ is given by

$$m := M - \frac{\mathrm{trace}(M)}{n} I\,. \tag{44}$$

Second, the extreme points of the base of $P(M)$ are lying on a sphere with center m and radius

$$r := \|M - \mathrm{trace}(M) v\,v^\top - m\| = \mathrm{trace}(M)\sqrt{1 - \frac{1}{n}}\,. \tag{45}$$

If the center m and radius r of a sphere in $\{A \in \mathrm{Sym}(k) : \mathrm{trace}(A) = 0\}$ are given the vertex M of the associated penumbra $P(M)$ is obtained by

$$M = m + \frac{r}{n} \frac{1}{\sqrt{1 - \frac{1}{n}}}\, I\,. \tag{46}$$

With this geometric interpretation in mind we may reformulate the task of finding a suitable maximal matrix $\overline{A}$ dominating the matrices $\{A_1, \ldots, A_m\}$: The *smallest* sphere enclosing the spheres associated with $\{A_1, \ldots, A_m\}$ determines the matrix $\overline{A}$ that dominates the A_i. It is minimal in the sense, that there is no smaller one w.r.t. the Loewner ordering which has this "covering property" of its penumbra. For each $i = 1, \ldots, m$, we sample within the set of extreme points $\{A_i - \mathrm{trace}(A_i) v\,v^\top\}$ of the base of $P(A_i)$ by expressing v in 3d-spherical coordinates, $v = (\sin\phi\cos\psi, \sin\phi\sin\psi, \cos\phi)$ with $\phi \in [0, 2\pi[, \psi \in [0, \pi[$. 'Vectorising' these matrices, that is, writing the entries of each of these matrices in a n^2-dimensional vector provides us with points for which a smallest enclosing ball has to be found. This is a non-trivial problem of computational geometry and we tackle it by using a sophisticated algorithm implemented by B. Gaertner [19]. The algorithm returns the center and the radius of the smallest enclosing ball from which we obtain with the help of the relations (44) – (46) the corresponding maximal matrix $\overline{A}$. As in (42) we set

$$\inf(A_1, \ldots, A_m) = -\sup(-A_1, \ldots, -A_m)\,. \tag{47}$$

As a consequence the notion of dilation/erosion and with them many other morphological operations are available now for matrix fields.

In the next section we turn to the PDE-based approach to dilation and erosion in the matrix setting.

4 PDE-Based Morphology for Matrix Fields

In order to find the matrix-valued counterparts of the scalar morphological PDEs (4) it is necessary to establish a rudimentary calculus for fields of symmetric matrices. For a more extended calculus for matrix fields the reader is referred to [13, 14].

4.1 Matrix-valued PDEs for dilation and erosion

The nonlinear PDEs (4) create a dilation and erosion process corresponding to a ball-shaped SE for grey value images. These equations contain the gradient operator $\nabla := (\partial_x, \partial_y, \partial_z)^\top$ with its partial derivatives and the Euclidean vector norm $\|(v_1, v_2, v_3)^\top\| := \sqrt{v_1^2 + v_2^2 + v_3^2}$. For both we have to find suitable analogs for matrices. To this end we have to clarify what a partial derivative, the absolute value and a square root of a symmetric matrix is. It is important *not* to consider a matrix norm as the extension of the vector norm in (4).

It is natural to define the equivalent $\overline{\partial}_\alpha$ of the partial derivative ∂_α, spatial ($\alpha \in \{x, y, z\}$) or temporal ($\alpha = t$), of a scalar function for a matrix-valued function $U(x, y, z, t) = (u_{i,j}(x, y, z, t))_{i,j=1,\ldots,n}$ by componentwise application of ∂_α:

$$\overline{\partial}_\alpha U := (\partial_\alpha u_{i,j})_{i,j=1,\ldots,n} \ . \tag{48}$$

Note that the subscript indicate the matrix components and not the grey value of an image u at pixel (ih_x, jh_y). Due to the linearity of matrix multiplication and differentiation the application of $\overline{\partial}_\alpha$ preserves symmetry, $U \in \mathrm{Sym}(k) \Longrightarrow \overline{\partial}_\alpha U \in \mathrm{Sym}(k)$, and is rotational invariant:
$\overline{\partial}_\alpha(WUW^\top) = W(\overline{\partial}_\alpha U)W^\top$ holds for any constant orthogonal matrix W.
With definition (32) the notion of a function of a symmetric matrix is already at our disposal. Hence, specifying the functions $h(x) = |x|^2$ and $h(x) = \sqrt{x}$ we have equipped the matrix-valued expression $\sqrt{|\overline{\partial}_x U|^2 + |\overline{\partial}_y U|^2 + |\overline{\partial}_z U|^2}$ with meaning. The latter is in fact a positive definite matrix if U is a non-constant matrix field, and it can be seen as a direct analog of the Euclidean norm of a vector.
Now we are in the position to establish the matrix-valued counterpart of (4):

$$\overline{\partial}_t U = \pm \sqrt{|\overline{\partial}_x U|^2 + |\overline{\partial}_y U|^2 + |\overline{\partial}_z U|^2} \, , \tag{49}$$

where "+" governs the dilation-like, and "−" rules the erosion-like evolution process.

4.2 Numerical schemes for matrix-valued PDEs of dilation and erosion

In order to solve the matrix-valued PDEs of dilation/erosion we transfer the numerical schemes OS-I, OS-II, and FCT presented in the previous section to the setting of matrix fields. Linear combinations and elementary functions such as the square, square-root or absolute value function for matrix fields are now at our disposal. Hence it is straightforward to define one sided differences in x-direction for 3D matrix fields of $k \times k$-matrices:

$$D_+^x U^n(i,j,k) := U^n((i+1)h_x, jh_y, kh_z) - U^n(ih_x, jh_y, kh_z) \in \mathrm{Sym}(k)\,, \quad (50)$$

$$D_-^x U^n(i,j,k) := U^n(ih_x, jh_y, kh_z) - U^n((i-1)h_x, jh_y, kh_z) \in \mathrm{Sym}(k)\,. \quad (51)$$

In order to avoid confusion with the subscript notation for matrix components we used the notation $U(i,j,k)$ to indicate the (matrix-) value of the matrix field evaluated at the voxel centred at $(ih_x, jh_y, kh_z) \in \mathbb{R}^3$. The central difference operator in x-direction is interpreted as

$$D_c^x U^n(i,j,k) := U^n((i+1)h_x, jh_x, kh_x) - U^n((i-1)h_x, jh_y, kh_z) \in \mathrm{Sym}(k) \quad (52)$$

The $y-$ and $z-$directions are treated accordingly. The notion of supremum and infimum of two matrices – as needed in a matrix variant of OS-I – has been provided by (34) and (35). However, care has to be taken for functions that are defined piecewise such as the minmod functions for two or three arguments. We generalise the minmod functions to the matrix setting by invoking the Loewner ordering

$$\mathrm{mm}(A_1, A_2) := \begin{cases} \inf(A_1, A_2) & \text{for} \quad A_1 > 0 \text{ and } A_2 > 0\,, \\ \sup(A_1, A_2) & \text{for} \quad A_1 < 0 \text{ and } A_2 < 0\,, \\ 0 & \quad \text{else}\,, \end{cases} \quad (53)$$

in the case of two matrices, while for three matrices we set

$$\mathrm{mm}(A_1, A_2, A_3) := \begin{cases} \inf_{opt}(A_1, A_2, A_3) & \text{for} \quad A_i > 0,\ i = 1,2,3\,, \\ \sup_{opt}(A_1, A_2, A_3) & \text{for} \quad A_1 < 0,\ i = 1,2,3\,, \\ 0 & \quad \text{else}\,, \end{cases} \quad (54)$$

with $\sup_{opt}$ and $\inf_{opt}$ given in (41) and (42).

Having these generalisations at our disposal the numerical schemes OS-I, OS-II, and finally the FCT scheme are available now in the setting of matrix fields.

The case differentiation necessary for shock filtering (11) is handled differently and utilises the *trace*-function: The sign of $\mathrm{tr}(\Delta_B U)$ of the matrix $\Delta_B U$ provides the switching mechanism for shock filtering in the matrix field setting.

5 Experimental Comparison of the Numerical Schemes

The hyperbolic morphological PDEs of dilation/erosion are numerically tackled with three specialised schemes: The first- and second-order schemes of Osher and Sethian (OS-I, OS-II) and the FCT scheme of Breuß and Weickert. We compare the results of basic morphological operations on images for ordering-based morphology and PDE-based methods obtained with the numerical schemes OS-I, OS-II and FCT. We restrict ourselves to the self-dual top hat (SDTH), the Beucher gradient, and the matrix-valued variant of a morphological Laplacian and shock filter. Note that the dilation and erosion are performed with respect to a *ball-shaped* structuring element. In extension of the experiments in [8] we first turn our attention to the scalar case in the next subsection.

5.1 Scalar valued data

In the scalar case we apply the morphological self-dual top hat and the Beucher gradient to the grey value test image of size 256×256 depicted in Figure 1.
We juxtapose the results of these operations when the underlying dilation/ erosion operations stem from the classical ordering-based definitions, or from the PDE-based approach with resolved with the three numerical schemes OS-I, OS-II, and FCT discussed above.
In the case of the self-dual top hat we performed 40 steps with time step size 0.1 resulting in an evolution time of 4 which corresponds to a ball with 4 pixel radius as SE. In Figure 2 we clearly see the superior performance of FCT when compared to OS-I and OS-II: The FCT-based SDTH selects the smaller details of the image almost as good as the ordering-based SDTH. Both OS-I and OS-II produce blurring artefacts due to the inherent numerical dissipation.
Let us now turn to the Beucher gradient ρ_B as our last example in the scalar setting. We performed 20 steps with time step size 0.1 resulting in an evolution time of 2 which corresponds to ball with 2 pixel radius as SE. The results displayed in Figure 3 confirm the advantage of the FCT scheme over the standard schemes. The edges are enhanced as in the ordering-based Beucher gradient while the schemes OS-I and OS-II suffer from blurring.

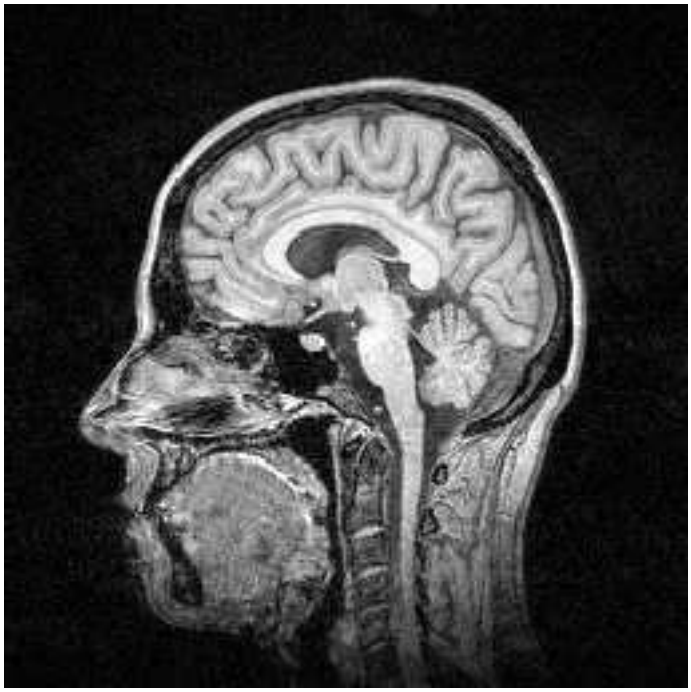

Figure 1: The grey value test image of size 256×256 used for the experiments in the scalar setting.

5.2 Matrix-valued data

In order to assess the quality of our numerical approach, we first show two experiments with matrix-valued data in two dimensions. Afterwards, a corresponding 3-D experiment is given.

In our first two numerical experiments for matrix data we use an artificial 20×20-field as well as an 128×128 slice of 3-D positive definite matrices originating from a 3-D DT-MRI data set of a human head, see figures 4, 6, 7, and 8.

The data are represented as ellipsoids via the level sets of the quadratic form $\{x^\top Ax : x \in \mathbb{R}^3\}$ associated with a matrix $A \in \mathrm{Sym}^+(3)$. Using A^{-2} the length of the semi-axes of the ellipsoid correspond directly with the three eigenvalues of the positive definite matrix.

The artificial data constitute a circular structure where the ellipsoids in the center are elongated, while those outside the circle are simple balls.

In Figure 5, the results with artificial test data are displayed. It is clearly visible that the ordering-based approach leads to sharp edges while the elongated tensors change their shape towards a round appearance. Note that the

sharp edges stem from a discrete approximation of the structuring element in the pixel grid. The PDE-based methods better preserve the initial shape of the tensors, but the Osher-Sethian approaches introduce numerical blurring of the edges. The FCT scheme performs better with this respect. The small tensors near the edges arise by geometrical effects as the structuring element is a perfect ball given by the Euclidean norm.
Exactly the analogous numerical behaviour is observable in our experiment with real-world data shown in Figure 6. The same assertion applies with respect to Figure 7. However, in the latter experiment, it becomes even clearer than in Figure 5 that the ordering-based approach and the PDE-based approach in the matrix-valued setting are not equivalent and thus cannot be expected to yield the same results.
In our last experiment in two dimensions we investigate the shock filter. For this morphological operation the differences between the numerical schemes are hardly visible. We included this example in order to show that it depends on the underlying process of interest if it pays off to use a high-resolution-type scheme.
In our last experiment, we show that the schemes for matrix-valued morphology can also be applied in three dimensions. Figure 9 shows that the qualitative behaviour of the FCT scheme worked out before carries over to the 3-D setting.

6 Conclusion

In this work we were concerned with numerical solution schemes for the morphological PDEs for dilation and erosion in the setting of matrix fields. It has been demonstrated that, firstly, it is possible to extend even sophisticated high-resolution schemes for morphological PDEs, such as the FCT, in a rather straightforward manner once the suitable matrix-algebraic foundations a properly prepared. Secondly, we showed in experiments that the use of a computational more expensive FCT indeed pays off in the matrix setting: It preserves or enhances edges and contours in matrix fields transformed with top-hats, morphological derivatives and shock filters better than the first or even second order schemes of Osher and Sethian. The findings reported on in this work confirm that the elaborate numerical machinery for PDE-based scalar morphology is now at our disposal for matrix-valued morphology as well.

References

[1] L. Alvarez and L. Mazorra. Signal and image restoration using shock filters and anisotropic diffusion. *SIAM Journal on Numerical Analysis*, 31:590–605, 1994.

[2] A. Barvinok. *A Course in Convexity*, volume 54 of *Graduate Studies in Mathematics*. American Mathematical Society, Providence, 2002.

[3] P. J. Basser, J. Mattiello, and D. LeBihan. MR diffusion tensor spectroscopy and imaging. *Biophysical Journal*, 66:259–267, 1994.

[4] J. Bigün, G. H. Granlund, and J. Wiklund. Multidimensional orientation estimation with applications to texture analysis and optical flow. *IEEE Transactions on Pattern Analysis and Machine Intelligence*, 13(8):775–790, August 1991.

[5] J. P. Boris and D. L. Book. Flux corrected transport. I. SHASTA, a fluid transport algorithm that works. *Journal of Computational Physics*, 11(1):38–69, 1973.

[6] J. P. Boris and D. L. Book. Flux corrected transport. III. Minimal error FCT algorithms. *Journal of Computational Physics*, 20:397–431, 1976.

[7] J. P. Boris, D. L. Book, and K. Hain. Flux corrected transport. II. Generalizations of the method. *Journal of Computational Physics*, 18:248–283, 1975.

[8] M. Breuß and J. Weickert. A shock-capturing algorithm for the differential equations of dilation and erosion. *Journal of Mathematical Imaging and Vision*, 25(2):187–201, September 2006.

[9] M. Breuß and M. Welk. Staircasing in semidiscrete stabilised inverse diffusion algorithms. *Journal of Computational and Applied Mathematics*, 206(1):520–533, 2007.

[10] B. Burgeth, A. Bruhn, S. Didas, J. Weickert, and M. Welk. Morphology for tensor data: Ordering versus PDE-based approach. *Image and Vision Computing*, 25(4):496–511, 2007.

[11] B. Burgeth, A. Bruhn, N. Papenberg, M. Welk, and J. Weickert. Mathematical morphology for matrix fields induced by the Loewner ordering in higher dimensions. *Signal Processing*, 87(2):277–290, 2007.

[12] B. Burgeth, A. Bruhn, N. Papenberg, M. Welk, and J. Weickert. Mathematical morphology for tensor data induced by the Loewner ordering in higher dimensions. *Signal Processing*, 87(2):277–290, February 2007.

[13] B. Burgeth, S. Didas, L. Florack, and J. Weickert. A generic approach to diffusion filtering of matrix-fields. *Computing*, 81:179–197, 2007.

[14] B. Burgeth, S. Didas, L. Florack, and J. Weickert. A generic approach to the filtering of matrix fields with singular PDEs. In F. Sgallari, F. Murli, and N. Paragios, editors, *Scale Space and Variational Methods in Computer Vision*, volume 4485 of *Lecture Notes in Computer Science*, pages 556–567. Springer, Berlin, 2007.

[15] B. Burgeth, N. Papenberg, A. Bruhn, M. Welk, C. Feddern, and J. Weickert. Morphology for higher-dimensional tensor data via Loewner ordering. In C. Ronse, L. Najman, and E. Decencière, editors, *Mathematical Morphology: 40 Years On*, volume 30 of *Computational Imaging and Vision*, pages 407–418. Springer, Dordrecht, 2005.

[16] L. C. Evans. *Partial Differential Equations*, volume 19 of *Graduate Studies in Mathematics*. American Mathematical Society, Providence, 1998.

[17] S. J. Farlow. *Partial Differential Equations for Scientists and Engineers*. Dover, New York, 1993.

[18] W. Förstner and E. Gülch. A fast operator for detection and precise location of distinct points, corners and centres of circular features. In *Proc. ISPRS Intercommission Conference on Fast Processing of Photogrammetric Data*, pages 281–305, Interlaken, Switzerland, June 1987.

[19] B. Gärtner. http://www.inf.ethz.ch/personal/gaertner. 2005.

[20] G. Gilboa, N. A. Sochen, and Y. Y. Zeevi. Regularized shock filters and complex diffusion. In A. Heyden, G. Sparr, M. Nielsen, and P. Johansen, editors, *Computer Vision – ECCV 2002*, volume 2350 of *Lecture Notes in Computer Science*, pages 399–413. Springer, Berlin, 2002.

[21] J. Goutsias, H. J. A. M. Heijmans, and K. Sivakumar. Morphological operators for image sequences. *Computer Vision and Image Understanding*, 62:326–346, 1995.

[22] J. Goutsias, L. Vincent, and D. S. Bloomberg, editors. *Mathematical Morphology and its Applications to Image and Signal Processing*,

volume 18 of *Computational Imaging and Vision*. Kluwer, Dordrecht, 2000.

[23] G. H. Granlund and H. Knutsson. *Signal Processing for Computer Vision*. Kluwer, Dordrecht, 1995.

[24] F. Guichard and J.-M. Morel. A note on two classical enhancement filters and their associated PDE's. *International Journal of Computer Vision*, 52(2/3):153–160, 2003.

[25] C. G. Harris and M. Stephens. A combined corner and edge detector. In *Proc. Fouth Alvey Vision Conference*, pages 147–152, Manchester, England, August 1988.

[26] H. J. A. M. Heijmans. *Morphological Image Operators*. Academic Press, Boston, 1994.

[27] H. J. A. M. Heijmans and J. B. T. M. Roerdink, editors. *Mathematical Morphology and its Applications to Image and Signal Processing*, volume 12 of *Computational Imaging and Vision*. Kluwer, Dordrecht, 1998.

[28] J.-B. Hiriart-Urruty and C. Lemarechal. *Fundamentals of Convex Analysis*. Springer, Heidelberg, 2001.

[29] R. A. Horn and C. R. Johnson. *Matrix Analysis*. Cambridge University Press, Cambridge, UK, 1990.

[30] H. P. Kramer and J. B. Bruckner. Iterations of a non-linear transformation for enhancement of digital images. *Pattern Recognition*, 7:53–58, 1975.

[31] R. J. LeVeque. *Finite Volume Methods for Hyperbolic Problems*. Cambridge University Press, Cambridge, UK, 2002.

[32] G. Louverdis, M. I. Vardavoulia, I. Andreadis, and P. Tsalides. A new approach to morphological color image processing. *Pattern Recognition*, 35:1733–1741, 2002.

[33] G. Matheron. *Eléments pour une théorie des milieux poreux*. Masson, Paris, 1967.

[34] G. Matheron. *Random Sets and Integral Geometry*. Wiley, New York, 1975.

[35] S. Osher and R. P. Fedkiw. *Level Set Methods and Dynamic Implicit Surfaces*, volume 153 of *Applied Mathematical Sciences*. Springer, New York, 2002.

[36] S. Osher and L. Rudin. Shocks and other nonlinear filtering applied to image processing. In A. G. Tescher, editor, *Applications of Digital Image Processing XIV*, volume 1567 of *Proceedings of SPIE*, pages 414–431. SPIE Press, Bellingham, 1991.

[37] S. Osher and L. I. Rudin. Feature-oriented image enhancement using shock filters. *SIAM Journal on Numerical Analysis*, 27:919–940, 1990.

[38] S. Osher and J. A. Sethian. Fronts propagating with curvature-dependent speed: Algorithms based on Hamilton–Jacobi formulations. *Journal of Computational Physics*, 79:12–49, 1988.

[39] C. Pierpaoli, P. Jezzard, P. J. Basser, A. Barnett, and G. Di Chiro. Diffusion tensor MR imaging of the human brain. *Radiology*, 201(3):637–648, December 1996.

[40] A. R. Rao and B. G. Schunck. Computing oriented texture fields. *CVGIP: Graphical Models and Image Processing*, 53:157–185, 1991.

[41] L. Remaki and M. Cheriet. Numerical schemes of shock filter models for image enhancement and restoration. *Journal of Mathematical Imaging and Vision*, 18(2):153–160, March 2003.

[42] E. Rouy and A. Tourin. A viscosity solutions approach to shape-from-shading. *SIAM Journal on Numerical Analysis*, 29:867–884, 1992.

[43] G. Sapiro. *Geometric Partial Differential Equations and Image Analysis*. Cambridge University Press, Cambridge, UK, 2001.

[44] G. Sapiro, R. Kimmel, D. Shaked, B. B. Kimia, and A. M. Bruckstein. Implementing continuous-scale morphology via curve evolution. *Pattern Recognition*, 26:1363–1372, 1993.

[45] J. G. M. Schavemaker, M. J. T. Reinders, and R. van den Boomgaard. Image sharpening by morphological filtering. In *Proc. 1997 IEEE Workshop on Nonlinear Signal and Image Processing*, Mackinac Island, MI, September 1997. www.ecn.purdue.edu/NSIP/.

[46] J. Serra. *Echantillonnage et estimation des phénomènes de transition minier*. PhD thesis, University of Nancy, France, 1967.

[47] J. Serra. *Image Analysis and Mathematical Morphology*, volume 1. Academic Press, London, 1982.

[48] J. Serra. *Image Analysis and Mathematical Morphology*, volume 2. Academic Press, London, 1988.

[49] J. A. Sethian. *Level Set Methods and Fast Marching Methods*. Cambridge University Press, Cambridge, UK, second edition, 1999. Paperback edition.

[50] K. Siddiqi, B. B. Kimia, and C.-W. Shu. Geometric shock-capturing ENO schemes for subpixel interpolation, computation and curve evolution. *Graphical Models and Image Processing*, 59:278–301, 1997.

[51] P. Soille. *Morphological Image Analysis*. Springer, Berlin, second edition, 2003.

[52] P. Stoll, C.-W. Shu, and B. B. Kimia. Shock-capturing numerical methods for viscosity solutions of certain PDEs in computer vision: The Godunov, Osher–Sethian and ENO schemes. Technical Report LEMS-132, Division of Engineering, Brown University, Providence, RI, 1994.

[53] H. Talbot and R. Beare, editors. *Proc. Sixth International Symposium on Mathematical Morphology and its Applications*. CSIRO Publishing, Sydney, Australia, April 2002. http://www.cmis.csiro.au/ismm2002/proceedings/.

[54] R. van den Boomgaard. Numerical solution schemes for continuous-scale morphology. In M. Nielsen, P. Johansen, O. F. Olsen, and J. Weickert, editors, *Scale-Space Theories in Computer Vision*, volume 1682 of *Lecture Notes in Computer Science*, pages 199–210. Springer, Berlin, 1999.

[55] L. J. van Vliet, I. T. Young, and A. L. D. Beckers. A nonlinear Laplace operator as edge detector in noisy images. *Computer Vision, Graphics and Image Processing*, 45(2):167–195, 1989.

[56] J. Weickert. Coherence-enhancing shock filters. In B. Michaelis and G. Krell, editors, *Pattern Recognition*, volume 2781 of *Lecture Notes in Computer Science*, pages 1–8. Springer, Berlin, 2003.

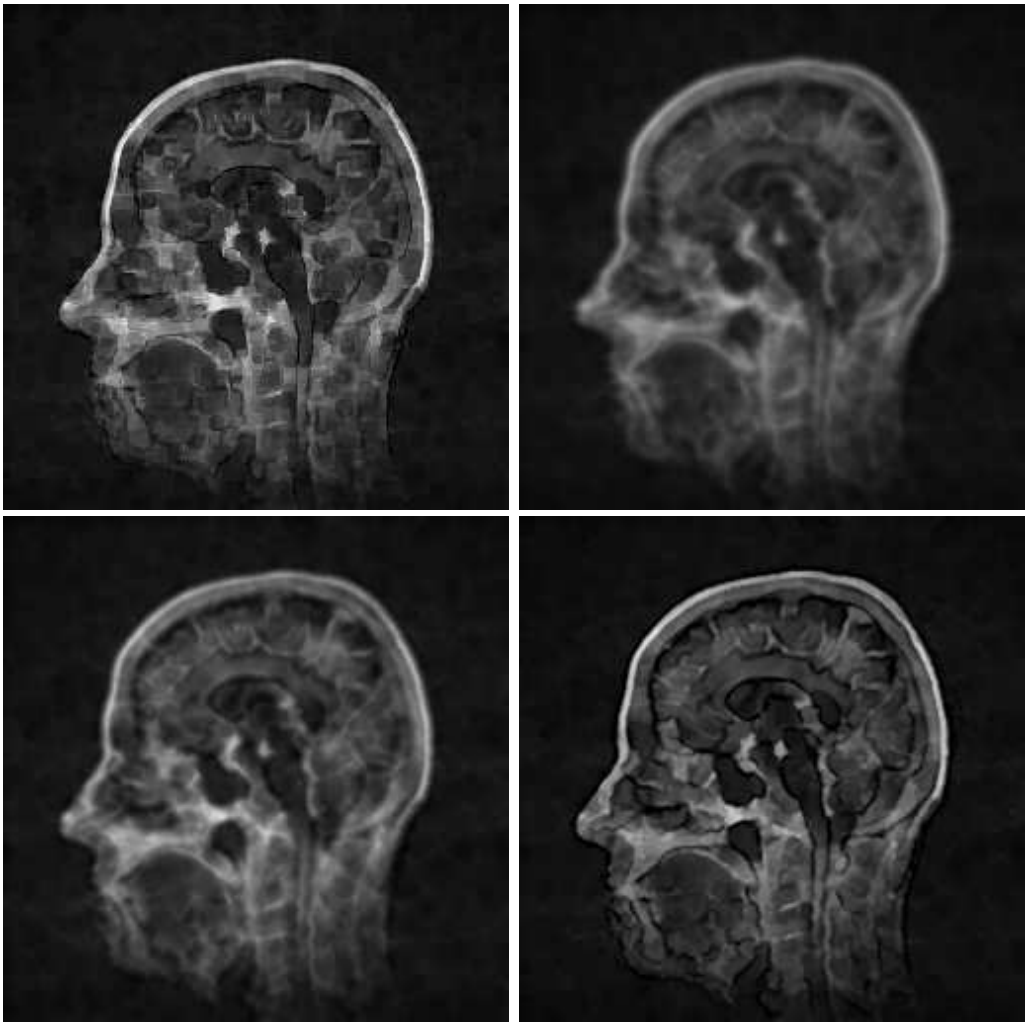

Figure 2: **Top left**: Ordering-based SDTH with ball-shaped SE of size 4. **Top right**: PDE-based SDTH via OS-I with time step size 0.1 and total evolution time 4. **Bottom left**: The same with OS-II. **Bottom right**: The same with FCT scheme.

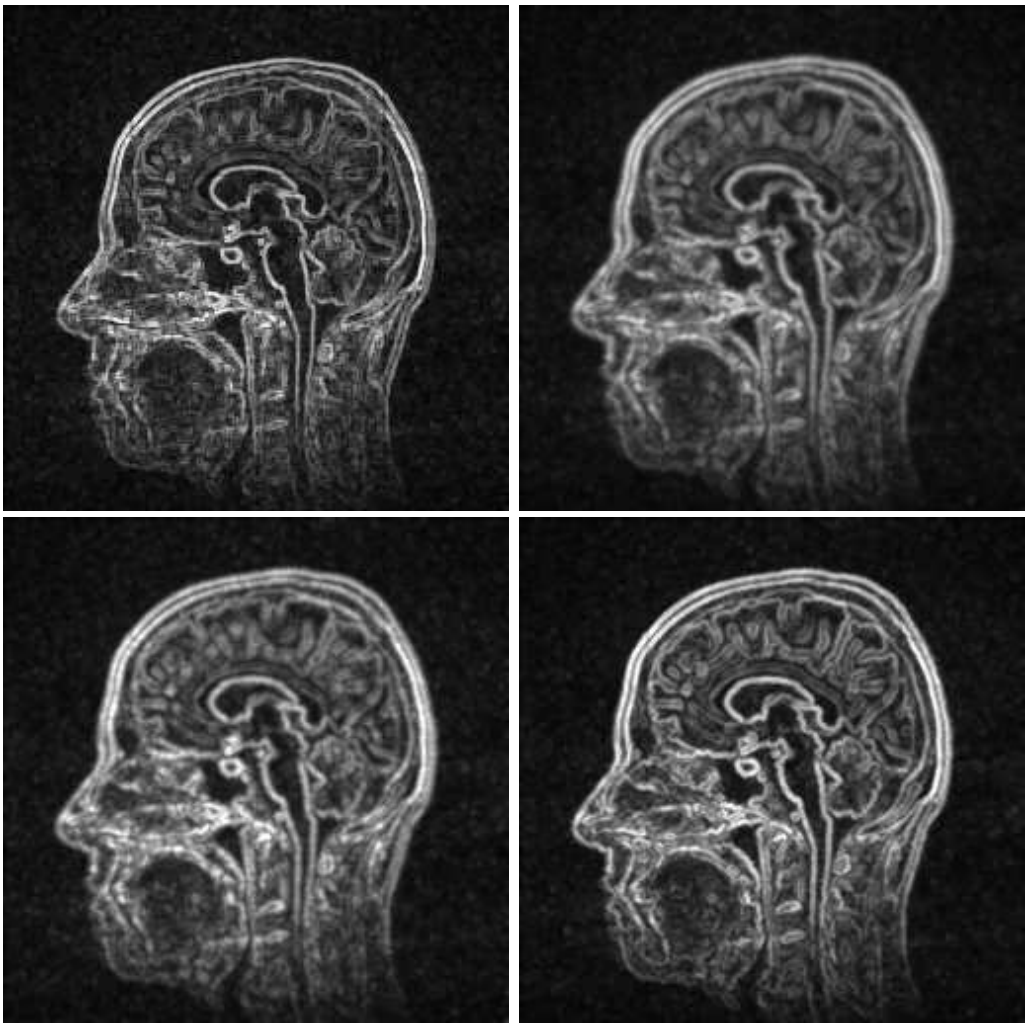

Figure 3: **Top left**: Ordering-based Beucher gradient with ball-shaped SE of size 2. **Top right**: PDE-based Beucher gradient via OS-I with time step size 0.1 and total evolution time 2. **Bottom left**: The same with OS-II. **Bottom right**: The same with FCT scheme.

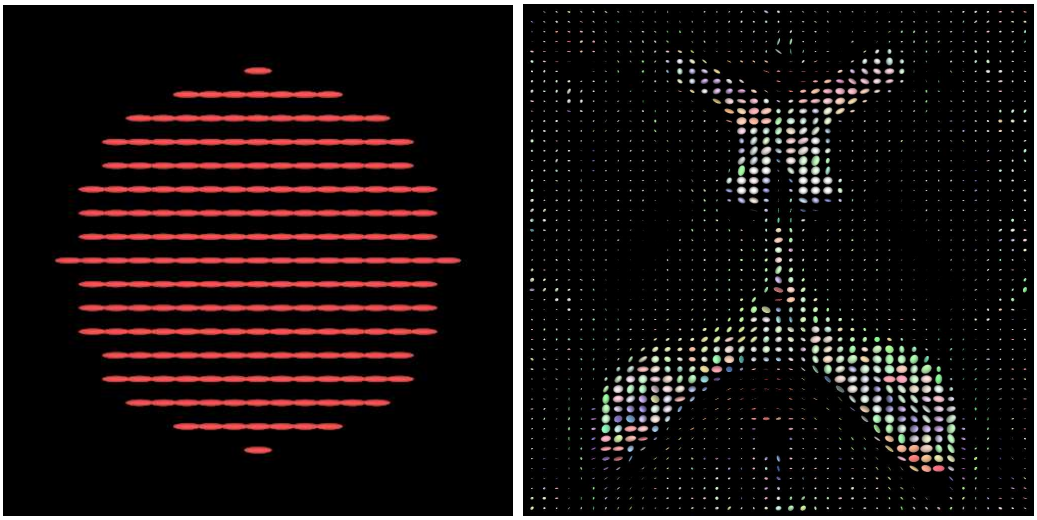

Figure 4: **Left**: Artificial matrix field. **Right**: 2D-slice of a real 3D DT-MRI data set.

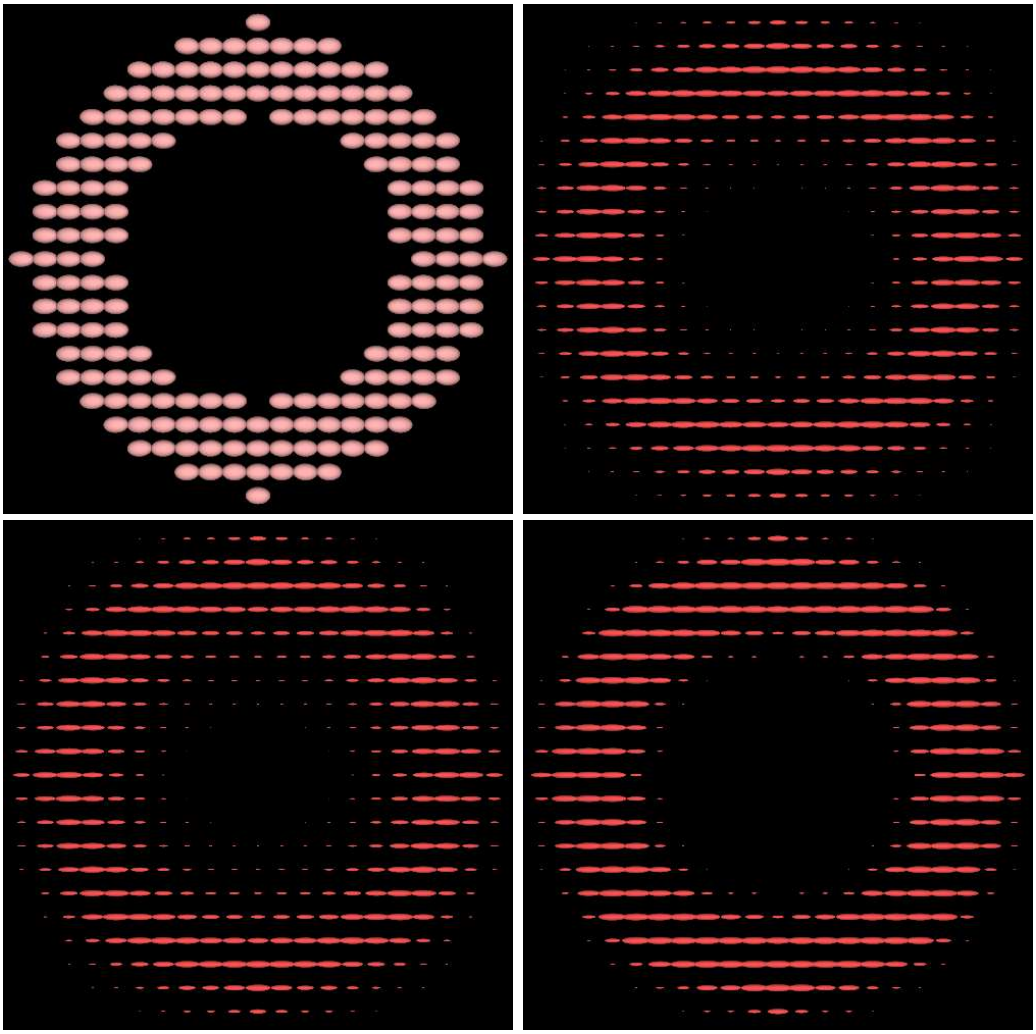

Figure 5: **Top left**: Ordering-based Beucher gradient with ball-shaped SE of size 2. **Top right**: PDE-based Beucher gradient via OS-I with time step size 0.1 and total evolution time 2. **Bottom left**: The same with OS-II. **Bottom right**: The same with FCT scheme.

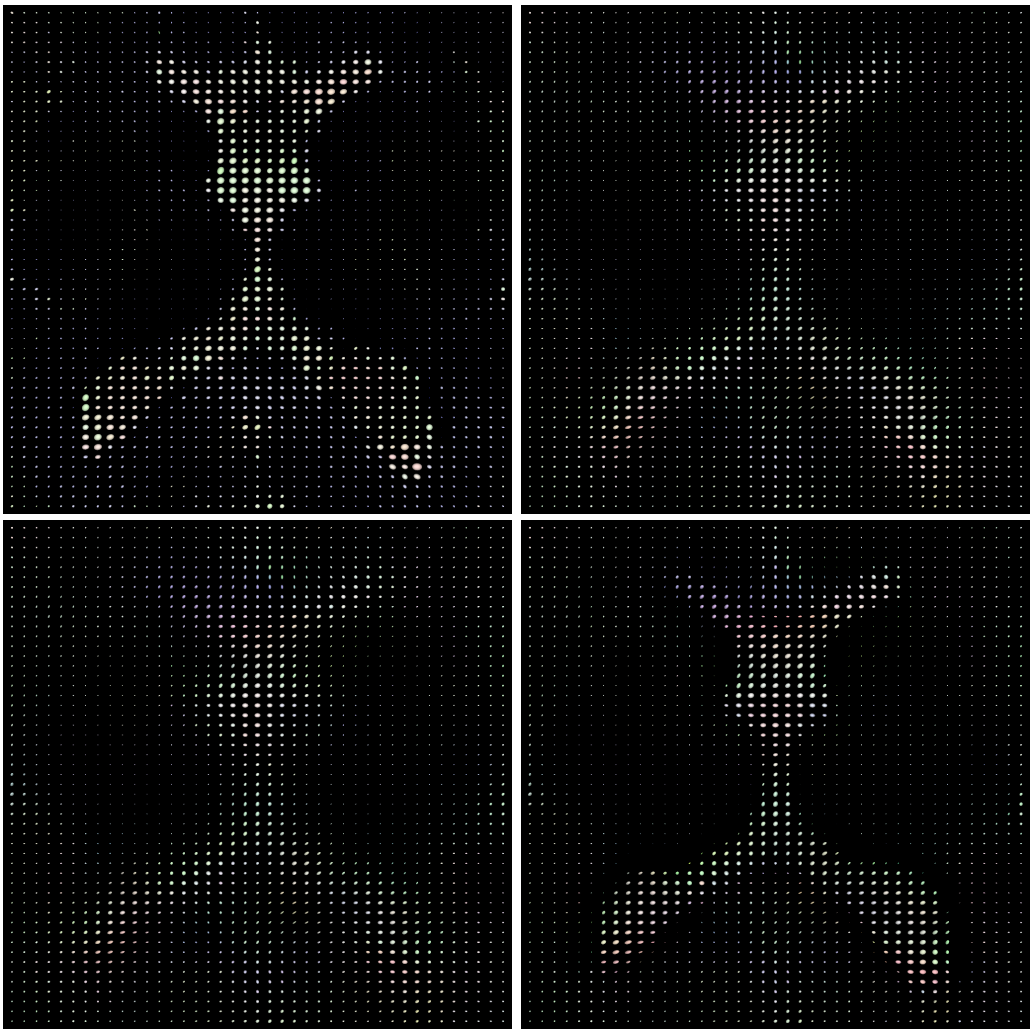

Figure 6: **Top left**: Ordering-based SDTH with ball-shaped SE of size 3. **Top right**: PDE-based SDTH via OS-I with time step size 0.1 and total evolution time 3. **Bottom left**: The same with OS-II. **Bottom right**: The same with FCT scheme.

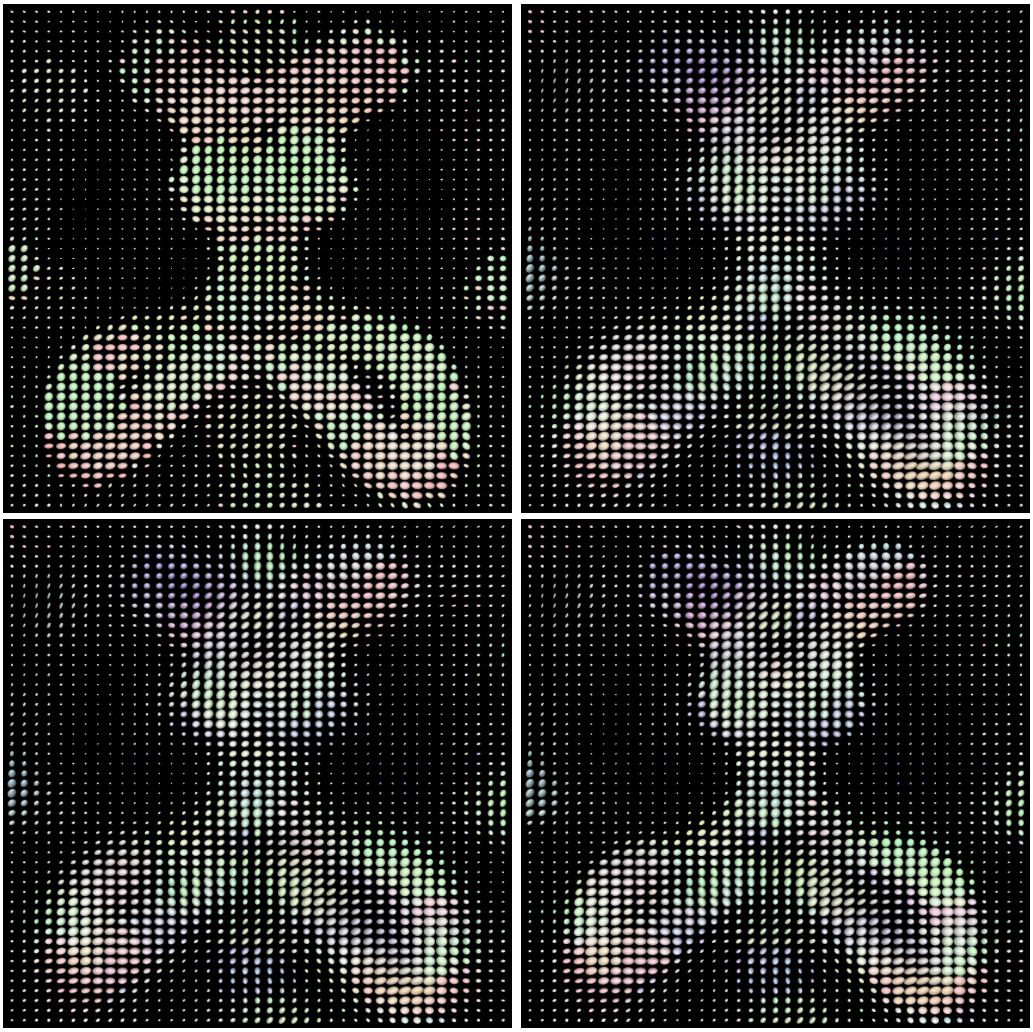

Figure 7: **Top left**: Ordering-based Beucher gradient with ball-shaped SE of size 3. **Top right**: PDE-based Beucher gradient via OS-I with time step size 0.1 and total evolution time 3. **Bottom left**: The same with OS-II. **Bottom right**: The same with FCT scheme.

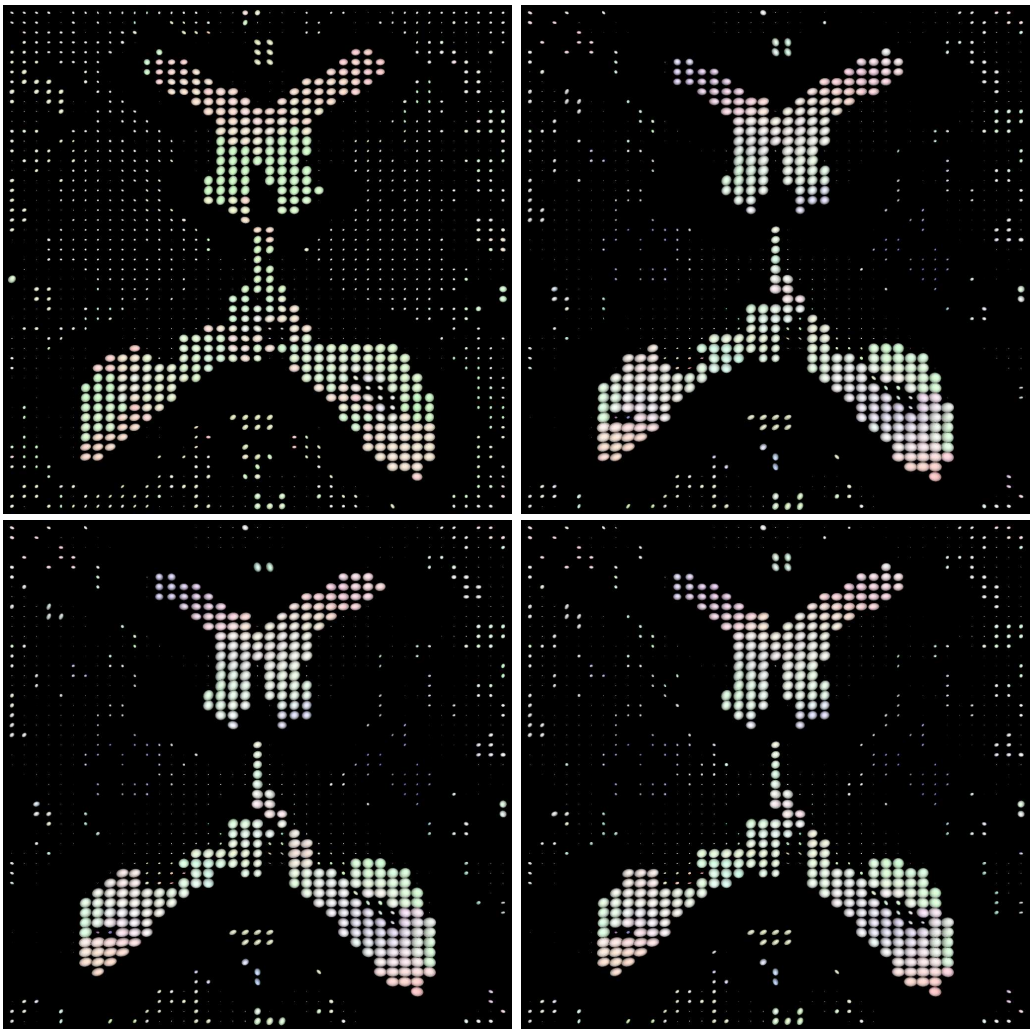

Figure 8: **Top left**: Ordering-based shock filter with ball-shaped SE of size 3. **Top right**: PDE-based shock filter via OS-I with time step size 0.1 and total evolution time 3. **Bottom left**: The same with OS-II. **Bottom right**: The same with FCT scheme.

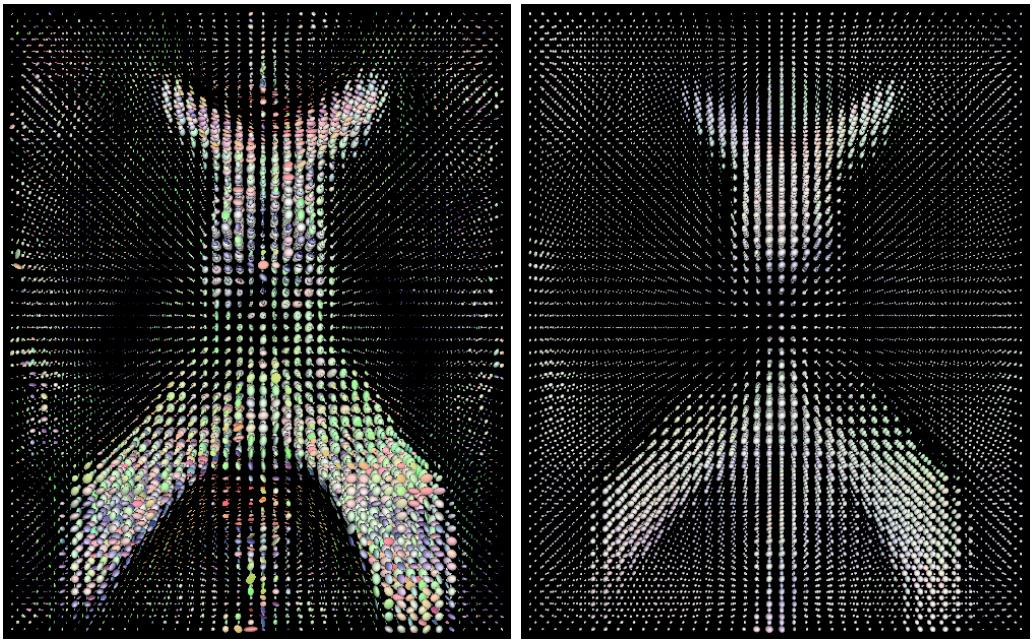

Figure 9: **Left**: Real-world 3-D matrix-valued of size $40 \times 50 \times 5$ voxels. **Right**: PDE-based self-dual top hat via FCT scheme with time step size 0.1 and total evolution time 3.